

Thermodynamics of the $S = 1/2$ maple-leaf Heisenberg antiferromagnet

Taras Hutak^{1,*}

¹*Institute for Condensed Matter Physics, National Academy of Sciences of Ukraine, Svientsitskii Street 1, 79011 L'viv, Ukraine*
(Dated: June 11, 2025)

The Heisenberg antiferromagnet on the maple-leaf lattice has recently gathered a great deal of attention. Competition between three non-equivalent bond interactions results in various ground-state quantum phases, the exact dimer-product singlet ground state being among them. The thermodynamic properties of this model are much less understood. We used high-temperature expansion up to the 18th order to study the thermodynamics of the $S = 1/2$ Heisenberg model on the uniform maple-leaf lattice with the ground state exhibiting a six-sublattice 120° long-range magnetic order. Padé approximants allow us to get reliable results up to the temperatures of about $T \approx 0.4$. To study thermodynamics for arbitrary temperatures, we made the interpolation using the entropy method. Based on the analysis of close Padé approximants, we find ground-state energy $e_0 = -0.53064\dots -0.53023$ in good agreement with numerical results. The specific heat $c(T)$ has a typical maximum at rather low temperatures $T \approx 0.379$ and the uniform susceptibility $\chi(T)$ at $T \approx 0.49$. We also estimate the value of $\chi(T)$ at zero temperature $\chi_0 \approx 0.05\dots 0.06$. The ground-state order manifests itself in the divergence of the so-called generalized Wilson ratio.

I. INTRODUCTION

The Heisenberg antiferromagnetic model on geometrically frustrated lattices is a fruitful playground for studying exotic classical and quantum magnetic phases [1, 2]. Two-dimensional antiferromagnets are of exceptional interest due to their low dimensionality and strong effects of quantum fluctuations. Usually, quantum fluctuations weaken classical long-range magnetic order (for example, this manifests in the reduction of the sublattice magnetization compared to the classical one). However, for some geometrically frustrated lattices, magnetic ordering can be suppressed completely [3]. The most famous and studied examples of such systems are the triangular- and kagome-lattice Heisenberg antiferromagnets. The former model exhibits long-range 120° magnetic order in the ground state [4, 5], whilst the latter ground state is now considered to be a quantum spin liquid [6, 7].

Another geometrically frustrated lattice of recent interest is the maple-leaf lattice [8]. Unlike triangular and kagome lattices, it has three non-equivalent bond types: bonds on hexagons, bonds on triangles, and the remaining bonds called dimer bonds, see Fig. 1. Mainly, the previous studies concerned ground-state behavior, such as phase diagrams and the magnetization process [9–22]. The most examined line on the parameter space of the general three types of nearest neighbor interactions is the $J-J_d$ model with equal exchange interactions on triangles and hexagons $J_h = J_t = J$. When interaction on the dimer bonds $J_d = 0$, one faces the bounce lattice, and $J_d = J$ corresponds to the maple-leaf lattice. One of the interesting features of this model is the case $J_d \geq 2J$ when the model hosts the exact dimer-product singlet ground state [11, 14] (together with the Shuistry–Sutherland lattice [23] of coordination number $z = 5$ these are the only two lattices in 2D possibly to host such a state [14]).

It was believed earlier that the increasing J_d drives the model to undergo a phase transition from the so-called canted 120° order at small and intermediate values of J_d to the dimer-singlet product state [11]. Recent numerical studies by the pseudo-fermion functional renormalization group [16] and density matrix renormalization group [20] show evidence of an intermediate paramagnetic phase (again quite similar to the phase diagram of the Shasty-Sutherland model [24]).

In the present paper, we will focus on the thermodynamic properties of the $S = 1/2$ uniform maple-leaf lattice Heisenberg antiferromagnetic model, where all non-equivalent bond interactions are equal. In this peculiar case, the ground state is the classical six-sublattice 120° magnetic order, or a staggered vector chirality order [25, 26], significantly weakened by quantum fluctuations and geometrical frustration of lattice. As a result, the model has one of the smallest sublattice magnetizations among the other Archimedean lattices [12, 13]. Although usually overshadowed by the fascinating ground-state behavior of the frustrated magnets, finite-temperature properties may also provide valuable insights even into ground-state physics [27, 28]. We will use the high-temperature expansion (HTE) and the entropy method interpolation to study the finite-temperature properties, such as specific heat $c(T)$ and the uniform susceptibility $\chi(T)$.

In the broader context, the uniform maple-leaf lattice Heisenberg antiferromagnet ($z = 5$, weak magnetic order) can be viewed as an intermediate between triangular ($z = 6$, magnetically ordered) and kagome one ($z = 4$, no magnetic order). It is interesting to compare the thermodynamic properties of these systems. It has been known for a long time that the kagome- and triangular-lattice antiferromagnets' specific heat shows an intriguing low-temperature behavior. For the kagome-lattice, both finite-temperature Lanczos [29] and entropy method results [30] confirm that the $c(T)$ has a low-temperature shoulder. On the contrary, the specific heat profile of the triangular lattice is less settled. Tensor network [31] and

* t.hutak@icmp.lviv.ua

finite-temperature Lanczos [32] indicate possible two energy scale physics display itself in the two-peak profile of $c(T)$, and entropy method results show one broad maximum [33].

Concerning materials, up to date, several natural minerals and synthesized compounds with maple-leaf lattice geometry are known [25, 26, 34–40]. However, studying some of them requires considering the Heisenberg model with higher spin $S > 1/2$. The relevant Heisenberg models for $S = 1/2$ materials are complex, and adequate description inevitably involves considering multiple exchange interaction types.

The paper is organized as follows. We begin with a description of the Model and Methods used in Sec. II. Results are reported in Sec. III, followed by the Conclusion in Sec. IV.

II. MODEL AND METHODS

The maple-leaf lattice can be viewed as a $1/7$ site-depleted (or a $1/6$ bond-depleted) triangular lattice [8]. The lattice has a coordination number $z = 5$ with six equivalent sites in a unit cell, and each site belongs to four bonds on triangles and one hexagon bond, see Fig. 1. We consider the isotropic Heisenberg Hamiltonian on the uniform maple-leaf lattice

$$\mathcal{H} = \sum_{\langle \mathbf{m}\alpha, \mathbf{n}\beta \rangle} \mathbf{S}_{\mathbf{m}\alpha} \cdot \mathbf{S}_{\mathbf{n}\beta}, \quad (1)$$

where the components of spin-1/2 operators $\mathbf{S}_{\mathbf{m}\alpha}$ are half of the Pauli matrices. The sum in Eq. (1) runs over the nearest neighbors' sites of the maple-leaf lattice defined by $\mathbf{R}_{\mathbf{m}\alpha} = \mathbf{R}_{\mathbf{m}} + \mathbf{r}_{\alpha}$. Here, $\mathbf{R}_{\mathbf{m}} = n_1 \mathbf{e}_1 + n_2 \mathbf{e}_2$ ($\{n_1, n_2\}$ are integers) generates lattice translations, where $\mathbf{e}_1 = \frac{1}{2}(5, \sqrt{3})$, $\mathbf{e}_2 = \frac{1}{2}(1, 3\sqrt{3})$ are lattice translation vectors, and \mathbf{r}_{α} , $\alpha = 1, \dots, 6$ are vectors defining the original position of the six equivalent sites in the unit cell: $\mathbf{r}_1 = (0, 0)$, $\mathbf{r}_2 = (1, 0)$, $\mathbf{r}_3 = (2, 0)$, $\mathbf{r}_4 = \frac{1}{2}(1, \sqrt{3})$, $\mathbf{r}_5 = \frac{1}{2}(3, \sqrt{3})$, $\mathbf{r}_6 = (1, \sqrt{3})$. We set the exchange interaction between the nearest neighbors $J = 1$, fixing the energy scale.

The model (1) has a six-sublattice 120° long-range magnetic order in the ground state. The angle between classical spins on triangles is $\pi/3$, the angle on hexagons is $5\pi/6$, and finally, on dimer bonds, the angle is $\pi/2$ [9, 10]. Long-range ground-state magnetic ordering in two dimensions leads to the low-temperature behavior of specific heat $c(T) \propto T^2$ (we will utilize this to make the interpolation using the entropy method).

To examine the thermodynamics of the model (1), we use the high-temperature expansion. HTE is a well-established technique for studying finite-temperature properties of quantum Heisenberg magnets [41]. Apart from being restricted only to some temperature range, this method is free from different limitations present in

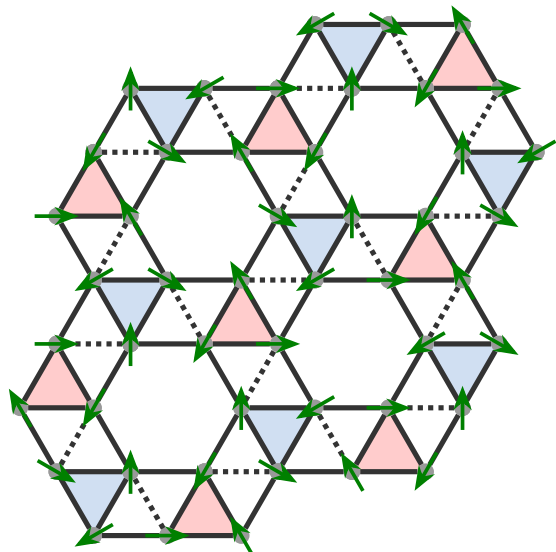


Figure 1. Maple-leaf lattice and the classical six-sublattice 120° ground-state magnetic order. The three nonequivalent interaction bonds are the bonds on hexagons, the bonds on triangles (shaded by blue and red colors), and the dimer bonds (dotted line). The angle between the classical spin on each bond is $5\pi/6$, $\pi/3$, and $\pi/2$, respectively [9, 10].

other numerical methods and allows the study of finite-temperature properties of the system in the thermodynamic limit. We used the algorithm of Pierre, Bernu, and Messio [42] to get the HTE of the logarithm of partition function $\ln Z$ up to 18th order over inverse temperature $\beta = 1/T$ [43],

$$\ln Z = \ln 2 + \frac{\theta^2}{2} + \frac{1}{6} \left[\sum_{j=0}^n \frac{a_j \beta^j}{(-4)^j j!} + \theta^2 \sum_{j=0}^{n-1} \frac{b_j \beta^j}{(-4)^j j!} \right], \quad (2)$$

where $\theta = \beta h/2$ and h is a longitudinal magnetic field. The obtained coefficients are reported in the Table I. Using the raw series (2), one can study thermodynamics in zero magnetic field (we will mainly focus on the specific heat $c(T) = \beta^2 [d^2 \ln Z / d\beta^2]$ and the uniform susceptibility $\chi(T) = 1/\beta [d^2 \ln Z / dh^2]$).

It is well known that the raw series can be improved by using Padé approximants $[u, d](\beta) = \mathcal{P}_u(\beta)/\mathcal{Q}_d(\beta)$, where $\mathcal{P}_u(\beta)$ and $\mathcal{Q}_d(\beta)$ are polynomials of u and d order, respectively, and series expansion around $\beta \rightarrow 0$ of $[u, d](\beta)$ reproduce the original series up to $u + d$ order. Usually, the raw HTE series breaks down at the temperatures of the order of the exchange interaction $T \approx J$. Padé approximants allow extending the region of validity to the intermediate temperatures $T \approx J/2$. However, for most models, especially for the frustrated magnets, the low-temperature regime is the most interesting one.

This obvious limitation of Padé approximants can be overstepped using the so-called entropy method to study thermodynamics on the whole temperature range [44–46]. This method was applied to the Heisenberg model

Table I. The high-temperature expansion series coefficients a_j, b_j of the $\ln Z$ obtained by the algorithm of [42].

n	a_j	b_j
0	0	0
1	-15	15
2	45	90
3	54	450
4	-1 458	1080
5	-9 720	9 240
6	219 240	587 088
7	3 801 168	8 502 096
8	-67 704 336	-154 746 240
9	-2 534 315 904	-5 666 092 416
10	31 633 948 800	105 282 266 880
11	2 572 904 353 536	6 877 641 769 728
12	-15 715 380 089 088	-82 970 518 557 696
13	-3 721 701 304 488 960	-10 929 337 956 185 088
14	-7 224 653 773 089 792	93 115 526 926 682 112
15	7 310 312 980 029 794 304	24 407 191 222 316 820 480
16	92 262 608 432 299 505 664	-133 859 693 794 581 970 944
17	-18 643 625 124 239 891 202 048	-77 080 129 995 065 123 438 592
18	-511 312 173 537 287 578 484 736	

on several frustrated lattices [30, 33, 47–52]. The idea of the entropy method is not to directly interpolate some observable, say, the specific heat, but the entropy $s(e)$ as a function of the internal energy e , guided by a knowledge of a low-temperature behavior. In this framework, all observables are defined parametrically on the interval $e \in [e_0, 0]$, where e_0 is a ground state energy,

$$T = \frac{1}{s'(e)}, \quad c = -\frac{[s'(e)]^2}{s''(e)}. \quad (3)$$

From the high-temperature expansion of the entropy $s(T)$, one can obtain the expansion of $s(e) = \ln 2 + \sum_{j=2}^n s_j e^j$ around $e_\infty = 0$ of the same order. To proceed further, the knowledge of the low-temperature behavior of $c(T)$ or the type of excitations is needed. In this paper, we consider only the case of a model with a gapless spectrum. In this scenario, the specific heat has a power-law form at low temperatures $c(T) \propto T^\alpha$. Using Eq. (3) one can immediately find out that such behavior of $c(T)$ leads to entropy $s(e) \propto (e - e_0)^{\alpha/(1+\alpha)}$.

Finally, to interpolate the entropy between high and low temperatures, we will use the auxiliary function $G(e)$ to remove possible problematic behavior of the $s'(e) = \beta$ in the ground state [45]

$$G(e) = \frac{[s(e)]^{\frac{1+\alpha}{\alpha}}}{e - e_0} \rightarrow G_{\text{app}}(e) = \frac{(\ln 2)^{\frac{\alpha}{1+\alpha}} \mathcal{P}_u(e)}{-e_0 \mathcal{Q}_d(e)}, \quad (4)$$

$$s_{\text{app}}(e) = [(e - e_0) G_{\text{app}}(e)]^{\frac{\alpha}{1+\alpha}}.$$

After the interpolation the entropy $s_{\text{app}}(e)$ can be recovered from the $G_{\text{app}}(e)$. Moreover, the value of the prefactor in $c(T) = AT^\alpha$ is $A_{\text{app}} = [\alpha^{1+\alpha}/(1+\alpha)^\alpha][G_{\text{app}}(e_0)]^\alpha$.

In the presence of a small magnetic field, the ground state energy of a gapless model is $e_0^h = e_0 - \chi_0 \frac{h^2}{2}$, where $\chi_0 \equiv \chi(T = 0)$ is the value of the uniform susceptibility at zero temperature. Assuming the value of χ_0 is known, we can now consider field-dependent entropy $s(e, h)$. After repeating the above-described procedure, we can also study the uniform susceptibility $\chi(T)$,

$$m = \frac{1}{[s'(e, h)]} \frac{\partial s(e, h)}{\partial h}, \quad \chi = \frac{m}{h}. \quad (5)$$

Thus, to study the thermodynamics of a gapless model in the framework of the entropy method, one needs to know the value of the ground-state energy e_0 , the power-law exponent of the specific heat at low temperatures α , and the value of the uniform susceptibility at zero temperature χ_0 . While e_0 can be found from the self-consistent procedure based on analysis of close Padé approximants and, in our case, $\alpha = 2$, the value of χ_0 is generally not known.

III. RESULTS

We begin a discussion of the thermodynamics of the $S = 1/2$ Heisenberg antiferromagnet on the maple-leaf lattice from the analysis of the simple Padé approximants. Results for the diagonal and close to diagonal Padé approximants from the 14th to 18th HTE order are reported in Fig. 2. The raw HTE series of the 18th order for the specific heat $c(T)$ and the uniform susceptibility $\chi(T)$ breaks down at temperatures about $T \approx 1$.

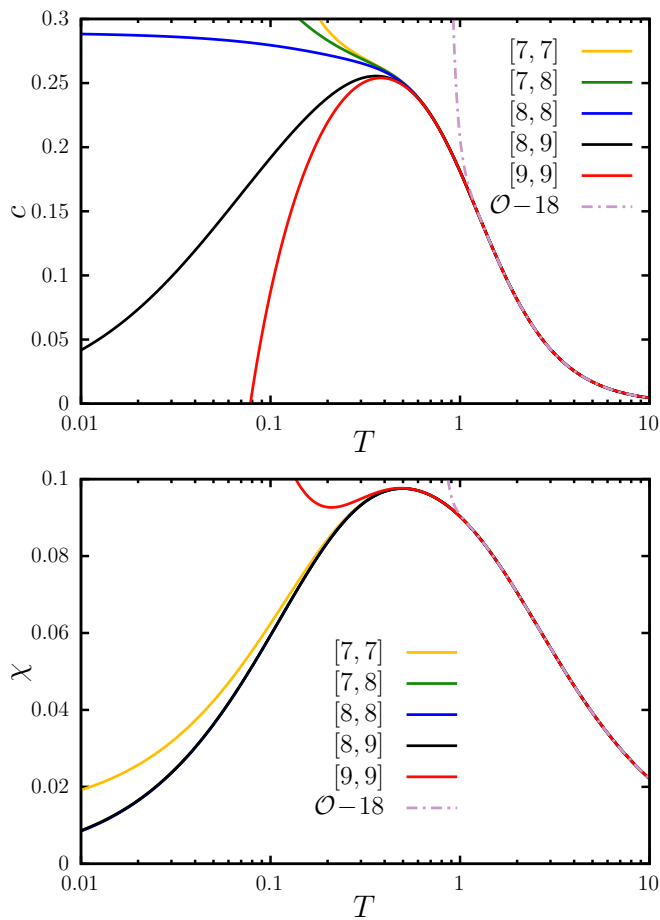


Figure 2. The specific heat $c(T)$ (top) and uniform susceptibility $\chi(T)$ (bottom) for the $S = 1/2$ antiferromagnetic Heisenberg model on the maple-leaf lattice. Close to diagonal and diagonal Padé approximants of HTE order from 14th to 18th are shown. Dashed curves on both panels correspond to the raw series of the 18th order.

By using simple Padé approximants, we can reach the temperature $T \approx 0.4$.

At present HTE order, we can not capture the maximum position of $c(T)$. Padé approximants of 18th and 17th order agree to the temperature $T \approx 0.4$, just slightly below the maximum. For the 18th-order Padé approximants (the diagonal one shown in Fig. 2 and a couple of the off-diagonal Padés), we have $T_{\max} \approx 0.38$ and $c(T_{\max}) \approx 0.254$. After integrating the convergent part of the specific heat, one can estimate the upper limit of the ground-state energy value $-\int_{0.4}^{\infty} dT c(T) \approx -0.456$, about 86% of the e_0 (see Table II). By utilizing another thermodynamic relation $\Delta s = \int_{0.4}^{\infty} dT c(T)/T \approx 0.347 \approx \ln 2/2$, we can see that down to temperature $T = 0.4$, about half of the total entropy is released. This indicates that the specific heat does not contain an additional low-temperature feature, as one should expect, considering that $c(T)$ recovered almost to its maximum position.

Contrary to the specific heat, the uniform susceptibility maximum is well captured by the Padé approximants

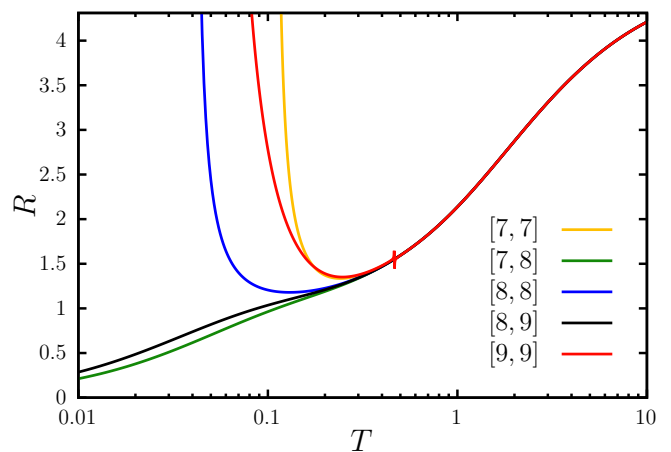


Figure 3. The generalized Wilson ratio $R(T)$ Eq. (6) at different HTE orders.

$T_{\max} \approx 0.497$ and $\chi(T_{\max}) \approx 0.097$. Approximants from the 15th to 17th order reported in Fig. 2 almost coincide.

Another useful quantity we can study for the 2D Heisenberg antiferromagnets using HTE is the so-called temperature-dependent generalized Wilson ratio [53, 54],

$$R(T) = \frac{4\pi^2 T \chi(T)}{3s(T)}. \quad (6)$$

This ratio was studied for the finite-size Heisenberg model systems for several 2D lattices [32, 53–57]. Contrary to its zero-temperature counterpart in the Fermi-liquid theory [58], it contains entropy $s(T)$ instead of the specific heat $c(T)$ in the denominator of Eq. (6), thus measuring the ratio of the density of the magnetic excitations (with $S_{\text{total}}^z > 0$) to the density of all excitations (including singlet excitations with $S_{\text{total}}^z = 0$).

The high-temperature limit of $R(T)$ for the isotropic Heisenberg model is $R|_{T \rightarrow \infty} = \pi^2/(3 \ln 2) \approx 4.746$. The most interesting is a low-temperature behavior. When low-temperature thermodynamics is dominated by singlet excitations, the generalized Wilson ratio tends to zero $R(T) \propto T^\eta \exp(-\Delta/T)$, where $\Delta = \Delta_t - \Delta_s$ is generally the difference between the triplet and singlet gap. Another scenario is when $R(T)$ tends to the finite value $R|_{T \rightarrow 0} \approx 1$, which indicates a gapless spin liquid state with spinon Fermi surfaces [53, 54]. But when the system has a long-range magnetic order in the ground state, as the model at hand, the uniform susceptibility has a finite non-zero value at zero temperature $\chi_0 > 0$, and magnon excitations produce entropy $s(T) \propto T^2$ at low temperatures. This results in the divergence of the generalized Wilson ratio at zero temperature $R(T) \propto T^{-1}$.

Padé approximants of different HTE orders for the generalized Wilson ratio are reported in Fig. 3. Clearly, for the considered model, one can not reach sufficiently low temperatures to get to the characteristic minimum of $R(T)$ (see, for example, numerical studies for Heisenberg antiferromagnets on the square and triangular lattices

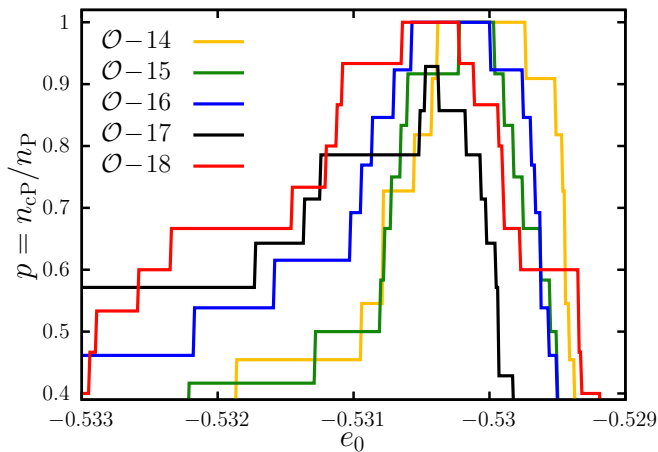


Figure 4. The ratio $p = n_{cP}/n_P$ of the number of close Padé approximants n_{cP} to the number of the initial set considered in the entropy method n_P , based on the series of 14th to 18th order as a function of the ground-state value e_0 .

[32, 56]) by using a simple Padé approximation. However, after a smooth decrease, diagonal Padé approximants from the 14th to 18th order reach a minimum at temperatures around $T < 0.3$, starting to increase rapidly after that, thus indicating the presence of the long-range magnetic order.

Now, let's turn to the entropy method interpolation. As one can see from Eq. (4), the interpolation requires the knowledge of both the ground-state energy e_0 and the low-temperature behavior of the specific heat. The low-temperature behavior of the $c(T)$ is governed by the antiferromagnetic spin-wave excitations and is known for the 2D antiferromagnets to be $c(T) \propto T^2$ [59]. The ground-state energy e_0 can be found based on the analysis of close (coinciding) Padé approximants [30]. This procedure was applied successfully to several Heisenberg antiferromagnets [30, 33, 50, 52]. Here, we will briefly describe the algorithm used in [52].

From now on, we will treat the ground-state energy e_0 as a parameter, and varying it with step 10^{-5} will check the closeness of the specific heat curves at a given value of e_0 . At the n th order, one can build $n + 1$ Padé approximants. From the start, we will dismiss four Padé approximants $[n, 0]$, $[n - 1, 1]$, $[1, n - 1]$, $[0, n]$ and form an initial set of $n - 3$ curves. The simple Padé approximants for the $c(T)$ start disagreeing at $T \approx 0.4$, so we evaluate $c(T)$ at a slightly higher temperature $T = 0.5$ and remove curves from the initial set which do not reproduce this value. After that, we slowly lower the temperature on each step eliminating the curves that differ from the mean value of the set by 0.001. At the end of this procedure, we end up with a bunch n_{cP} of very close Padé approximants at a given value of e_0 . The greater the number of remaining Padé approximants n_{cP} , the closer one gets to the correct ground state value e_0 [30].

The results of this search for the HTE order from 14th to 18th are shown in Fig. 4. At each order exists a short

Table II. Comparison of the ground-state energy values e_0 obtained by different methods.

ED ($N = 36$) [10]	-0.5389725
CCM [13]	-0.53094
iPEPS [21]	-0.530359
entropy method (this work)	-0.53064... - 0.53023
LSWT [10]	-0.5121574375

range of the ground state values where all Padé approximants are very close (the 17th order is an exception where all but one curve are very close). We see the tendency of e_0 very slowly moving to the lower values while increasing the order n . At the 18th order, the region where all curves are close is $e_0 = -0.53064 \dots - 0.53023$.

The ground-state energy value was studied by several methods: the exact diagonalization (ED) of the finite $N = 36$ system [10], the coupled cluster method (CCM) [11–13], the infinite projected entangled-pair state ansatz (iPEPS) [21], and the linear spin wave theory (LSWT) [10] (we also mention here the density matrix renormalization group study [20], where the value was not directly reported but differs very slightly from other numerics). The entropy method prediction agrees with these findings up to three significant digits, see Table II.

We now move on to the thermodynamic properties. We utilize ground-state values e_0 and use Eqs. (3) and (5) to study the specific heat $c(T)$, uniform susceptibility $\chi(T)$, and generalized Wilson ratio $R(T)$. These results are reported in Fig. 5 (we use $e_0 = -0.53044$, and all curves correspond to the [9, 9] Padé approximants).

The specific heat has one maximum at $T_{\max} \approx 0.379$ and $c(T_{\max}) \approx 0.254$, located at slightly lower temperatures than accessible by only using simple Padé approximants. In the framework of the entropy method, one can also calculate the prefactor in the low-temperature power-law of $c(T)$, in our case, $c(T) \approx 13.4T^2$. The dependence of the specific heat on the ground-state energy value and the HTE order is very weak for the range of e_0 where $p = p_{\max}$ (the obtained curves are almost indistinguishable).

The study of uniform susceptibility requires knowledge of its value at zero temperature χ_0 . Unfortunately, there is no available data on χ_0 in the literature. We can again use it as a parameter to correctly reproduce the maximum position of $\chi(T)$, captured by simple Padé approximants. Guided by this knowledge, we found that χ_0 belongs in the range $\chi_0 \approx 0.05 \dots 0.06$. The other choices of its value can spoil the correct intermediate-temperature behavior of the uniform susceptibility.

The generalized Wilson ratio shows typical behavior for the ordered antiferromagnetic systems [32, 56]. Slowly decreasing from its high-temperature value, it reaches a minimum at the temperature around $T \approx 0.16$ (depending on the chosen χ_0 value), starting after that increasing rapidly. $R(T)$ depends very slightly on the

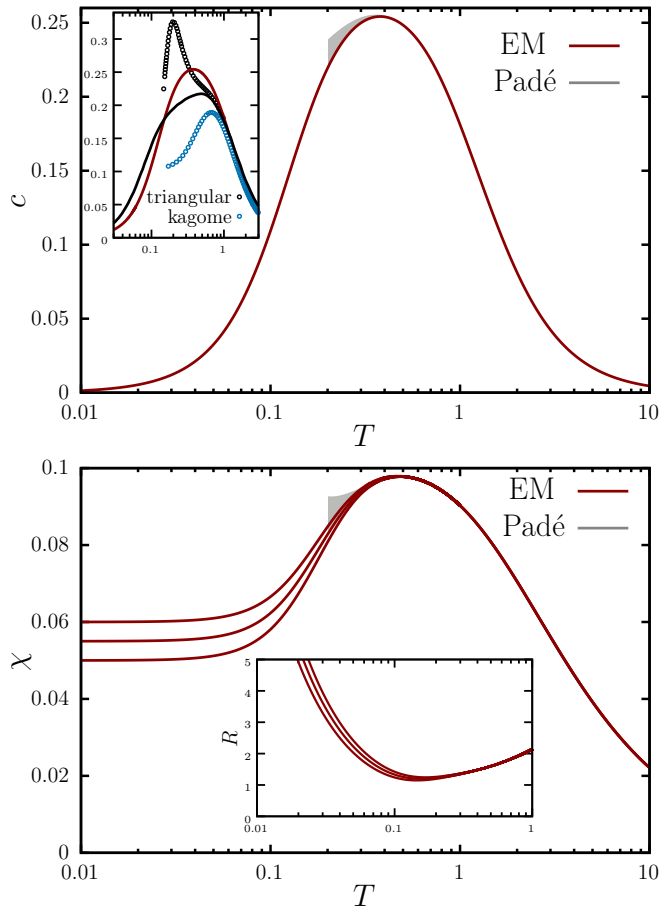


Figure 5. Entropy-method results for the specific heat $c(T)$ (top) and the uniform susceptibility $c(T)$ (bottom) of the $S = 1/2$ Heisenberg antiferromagnet on the maple-leaf lattice. The inset in the top figure offers a comparison of the maple-leaf $c(T)$ with the finite-system diagonalization for the triangular- and kagome-lattice models (empty circles, data taken from [32] and [29], respectively) and entropy method results (solid line, data taken from [33]). The generalized Wilson ratio $R(T)$ is shown in the bottom inset, assuming plausible values $\chi_0 = 0.05, 0.055, 0.06$. On both panels, the shaded grey area corresponds to the difference between simple Padé approximants [8, 9] and [9, 9].

particular choice of χ_0 , see the inset in the bottom panel of Fig. 5 data for $\chi_0 = 0.05, 0.055, 0.06$.

Finally, it is worth putting our studies in the context of two other frustrated systems mentioned in the Introduction, triangular- and kagome-lattice Heisenberg antiferromagnets, see the inset on the top panel in Fig. 5. The specific heat behavior of the maple-leaf antiferromagnet is quite similar to the one obtained by the entropy method for the triangular lattice [33] (likely, the additional low-temperature maximum for the $N = 36$ system is the finite-size effect). However, instead of a broad maximum for the triangular lattice, the maple-leaf

antiferromagnet $c(T)$ displays a higher maximum located at lower temperatures.

IV. CONCLUSION

In the present paper, we studied the thermodynamics of the $S = 1/2$ Heisenberg antiferromagnet on the uniform maple-leaf lattice based on the high-temperature series expansion up to the 18th order obtained using the algorithm of [42]. We discuss the thermodynamic properties of the specific heat $c(T)$, the uniform susceptibility $\chi(T)$, and the generalized Wilson ratio $R(T)$. Simple Padé approximation allows us to reach the temperatures $T \approx 0.4$. At this temperature, we can confidently determine the maximum position of the uniform susceptibility $T \approx 0.49$. However, the maximum position of the specific heat at this temperature is not reached yet.

To study finite-temperature properties at arbitrary temperatures, we used the entropy method. Based on the exact knowledge of the low-temperature behavior of the specific heat, we made an interpolation between high and low temperatures. Our main findings are the following. Using the procedure of finding ground-state energy based on the analysis of close (almost coinciding) Padé approximants, we found e_0 to be in a very narrow region $e_0 = -0.53064\dots - 0.53023$. The obtained e_0 value is in good agreement with recent numerical studies. The specific heat shows one maximum located at $T \approx 0.379$ just slightly lower than the temperatures reached by simple Padé approximants. We also predict the value of the uniform susceptibility at zero temperature $\chi_0 \approx 0.05\dots 0.06$. The specific heat behavior of the maple-leaf antiferromagnet is similar to the triangular lattice one, however, with a higher maximum located at lower temperatures.

ACKNOWLEDGEMENTS

I acknowledge the discussions with Johannes Richter at the early stages of the work and am grateful to Oleg Derzhko and Dmytro Yaremchuk for the fruitful discussions and for reading the manuscript. I also thank the authors of the paper [42] for making their algorithm open, and I am particularly grateful to Laura Messio for the valuable discussion about running the algorithm.

The work was supported by the fellowship of the National Academy of Sciences of Ukraine for young scholars, and by the Projects of research works of young scientists of the National Academy of Sciences of Ukraine (project # 29-04/18-2023, Frustrated quantum magnets at finite temperatures), as well as by the EURIZON project (#3025 "Frustrated quantum spin models to explain the properties of magnets over wide temperature range"), which is funded by the European Union under grant agreement No. 871072.

I am grateful to the Armed Forces of Ukraine for their protection during this study.

-
- [1] J. Knolle and R. Moessner, A Field Guide to Spin Liquids, *Annu. Rev. Condens. Matter Phys.* **10**, 451 (2019).
- [2] C. Broholm, R. J. Cava, S. A. Kivelson, D. G. Nocera, M. R. Norman, and T. Senthil, Quantum spin liquids, *Science* **367**, eaay0668 (2020).
- [3] J. Richter, J. Schulenburg, and A. Honecker, Quantum magnetism in two dimensions: From semi-classical Néel order to magnetic disorder, in *Quantum Magnetism*, edited by U. Schollwöck, J. Richter, D. J. J. Farnell, and R. F. Bishop (Springer Berlin Heidelberg, Berlin, Heidelberg, 2004) pp. 85–153.
- [4] L. Capriotti, A. E. Trumper, and S. Sorella, Long-Range Néel Order in the Triangular Heisenberg Model, *Phys. Rev. Lett.* **82**, 3899 (1999).
- [5] S. R. White and A. L. Chernyshev, Néel Order in Square and Triangular Lattice Heisenberg Models, *Phys. Rev. Lett.* **99**, 127004 (2007).
- [6] S. Yan, D. A. Huse, and S. R. White, Spin-Liquid Ground State of the $s = 1/2$ Kagome Heisenberg Antiferromagnet, *Science* **332**, 1173 (2011).
- [7] S. Depenbrock, I. P. McCulloch, and U. Schollwöck, Nature of the Spin-Liquid Ground State of the $S = 1/2$ Heisenberg Model on the Kagome Lattice, *Phys. Rev. Lett.* **109**, 067201 (2012).
- [8] D. D. Betts, A new two-dimensional lattice of coordination number five, *Proc. N. S. Inst. Sci.* **40**, 95 (1995).
- [9] J. Schulenburg, J. Richter, and D. D. Betts, Heisenberg Antiferromagnet on a $1/7$ -Depleted Triangular Lattice, *Acta Phys. Pol. A* **97**, 971 (2000).
- [10] D. Schmalfuß, P. Tomczak, J. Schulenburg, and J. Richter, The spin- $\frac{1}{2}$ Heisenberg antiferromagnet on a $\frac{1}{7}$ -depleted triangular lattice: Ground-state properties, *Phys. Rev. B* **65**, 224405 (2002).
- [11] D. J. J. Farnell, R. Darradi, R. Schmidt, and J. Richter, Spin-half Heisenberg antiferromagnet on two archimedean lattices: From the bounce lattice to the maple-leaf lattice and beyond, *Phys. Rev. B* **84**, 104406 (2011).
- [12] D. J. J. Farnell, O. Götzke, J. Richter, R. F. Bishop, and P. H. Y. Li, Quantum $s = \frac{1}{2}$ antiferromagnets on Archimedean lattices: The route from semiclassical magnetic order to nonmagnetic quantum states, *Phys. Rev. B* **89**, 184407 (2014).
- [13] D. J. J. Farnell, O. Götzke, J. Schulenburg, R. Zinke, R. F. Bishop, and P. H. Y. Li, Interplay between lattice topology, frustration, and spin quantum number in quantum antiferromagnets on Archimedean lattices, *Phys. Rev. B* **98**, 224402 (2018).
- [14] P. Ghosh, T. Müller, and R. Thomale, Another exact ground state of a two-dimensional quantum antiferromagnet, *Phys. Rev. B* **105**, L180412 (2022).
- [15] P. Ghosh, J. Seufert, T. Müller, F. Mila, and R. Thomale, Maple leaf antiferromagnet in a magnetic field, *Phys. Rev. B* **108**, L060406 (2023).
- [16] L. Gresista, C. Hickey, S. Trebst, and Y. Iqbal, Candidate quantum disordered intermediate phase in the Heisenberg antiferromagnet on the maple-leaf lattice, *Phys. Rev. B* **108**, L241116 (2023).
- [17] M. Gembé, L. Gresista, H.-J. Schmidt, C. Hickey, Y. Iqbal, and S. Trebst, Noncoplanar orders and quantum disordered states in maple-leaf antiferromagnets, *Phys. Rev. B* **110**, 085151 (2024).
- [18] J. Sonnenschein, A. Maity, C. Liu, R. Thomale, F. Ferrari, and Y. Iqbal, Candidate quantum spin liquids on the maple-leaf lattice, *Phys. Rev. B* **110**, 014414 (2024).
- [19] P. Ghosh, Triplon analysis of magnetic disorder and order in maple-leaf Heisenberg magnet, *J. Phys.: Condens. Matter* **36**, 455803 (2024).
- [20] J. Beck, J. Bodky, J. Motruk, T. Müller, R. Thomale, and P. Ghosh, Phase diagram of the $J-J_d$ Heisenberg model on the maple leaf lattice: Neural networks and density matrix renormalization group, *Phys. Rev. B* **109**, 184422 (2024).
- [21] P. Schmoll, J. Naumann, E. J., and Y. Iqbal, Bathing in a sea of candidate quantum spin liquids: From the gapless ruby to the gapped maple-leaf lattice (2024), arXiv:2407.07145.
- [22] P. Ghosh, Chiral crossroads in Ho_3ScO_6 : a tale of frustration in maple leaf lattice (2025), arXiv:2504.12387.
- [23] B. S. Shastry and B. Sutherland, Exact ground state of a quantum mechanical antiferromagnet, *Physica B+C* **108**, 1069 (1981).
- [24] P. Corboz, Y. Zhang, B. Ponsioen, and F. Mila, Quantum spin liquid phase in the Shastry-Sutherland model revealed by high-precision infinite projected entangled-pair states (2025), arXiv:2502.14091.
- [25] Y. Haraguchi, A. Matsuo, K. Kindo, and Z. Hiroi, Frustrated magnetism of the maple-leaf-lattice antiferromagnet $\text{MgMn}_3\text{O}_7 \cdot 3\text{H}_2\text{O}$, *Phys. Rev. B* **98**, 064412 (2018).
- [26] C. Aguilar-Maldonado, R. Feyerherm, K. Prokeš, L. Keller, and B. Lake, Structure and magnetic properties of the maple leaf antiferromagnet Ho_3ScO_6 , *Phys. Rev. B* **111**, 094439 (2025).
- [27] P. Popp, A. P. Ramirez, and S. Syzranov, Origin of the hidden energy scale and the f -ratio in geometrically frustrated magnets (2024), arXiv:2406.12966.
- [28] A. P. Ramirez and S. V. Syzranov, Short-range order and hidden energy scale in geometrically frustrated magnets, *Mater. Adv.* **6**, 1213 (2025).
- [29] J. Schnack, J. Schulenburg, and J. Richter, Magnetism of the $N = 42$ kagome lattice antiferromagnet, *Phys. Rev. B* **98**, 094423 (2018).
- [30] B. Bernu, L. Pierre, K. Essafi, and L. Messio, Effect of perturbations on the kagome $S = \frac{1}{2}$ antiferromagnet at all temperatures, *Phys. Rev. B* **101**, 140403 (2020).
- [31] L. Chen, D.-W. Qu, H. Li, B.-B. Chen, S.-S. Gong, J. von Delft, A. Weichselbaum, and W. Li, Two-temperature scales in the triangular-lattice Heisenberg antiferromagnet, *Phys. Rev. B* **99**, 140404 (2019).
- [32] M. Ulaga, J. Kokalj, A. Wietek, A. Zorko, and P. Prelovšek, Finite-temperature properties of the easy-axis Heisenberg model on frustrated lattices, *Phys. Rev. B* **109**, 035110 (2024).
- [33] M. G. Gonzalez, B. Bernu, L. Pierre, and L. Messio, Ground-state and thermodynamic properties of the spin- $\frac{1}{2}$ Heisenberg model on the anisotropic triangular lattice, *SciPost Phys.* **12**, 112 (2022).
- [34] T. Fennell, J. O. Piatek, R. A. Stephenson, G. J. Nilsen, and H. M. Rønnow, Spangolite: an $s = 1/2$ maple leaf lattice antiferromagnet?, *J. Phys.: Condens. Matter* **23**, 164201 (2011).
- [35] C. Venkatesh, B. Bandyopadhyay, A. Midya, K. Mahalingam, V. Ganesan, and P. Mandal, Magnetic proper-

- ties of the one-dimensional $S = \frac{3}{2}$ Heisenberg antiferromagnetic spin-chain compound $\text{Na}_2\text{Mn}_3\text{O}_7$, *Phys. Rev. B* **101**, 184429 (2020).
- [36] Y. Haraguchi, A. Matsuo, K. Kindo, and Z. Hiroi, Quantum antiferromagnet bluebellite comprising a maple-leaf lattice made of spin-1/2 Cu^{2+} ions, *Phys. Rev. B* **104**, 174439 (2021).
- [37] R. Makuta and C. Hotta, Dimensional reduction in quantum spin- $\frac{1}{2}$ system on a $\frac{1}{7}$ -depleted triangular lattice, *Phys. Rev. B* **104**, 224415 (2021).
- [38] B. Saha, A. K. Bera, S. M. Yusuf, and A. Hoser, Two-dimensional short-range spin-spin correlations in the layered spin- $\frac{3}{2}$ maple leaf lattice antiferromagnet $\text{Na}_2\text{Mn}_3\text{O}_7$ with crystal stacking disorder, *Phys. Rev. B* **107**, 064419 (2023).
- [39] P. Ghosh, T. Müller, Y. Iqbal, R. Thomale, and H. O. Jeschke, Effective spin-1 breathing kagome Hamiltonian induced by the exchange hierarchy in the maple leaf mineral bluebellite, *Phys. Rev. B* **110**, 094406 (2024).
- [40] P. Schmoll, H. O. Jeschke, and Y. Iqbal, *Tensor network analysis of the maple-leaf antiferromagnet spangolite* (2024), arXiv:2404.14905.
- [41] J. Oitmaa, C. Hamer, and W. Zheng, *Series expansion methods for strongly interacting lattice models* (Cambridge University Press, 2006).
- [42] L. Pierre, B. Bernu, and L. Messio, High temperature series expansions of $S = 1/2$ Heisenberg spin models: Algorithm to include the magnetic field with optimized complexity, *SciPost Phys.* **17**, 105 (2024).
- [43] We mention here that Eq. (2) is a small h expansion of the Eq. 16 in [42].
- [44] B. Bernu and G. Misguich, Specific heat and high-temperature series of lattice models: Interpolation scheme and examples on quantum spin systems in one and two dimensions, *Phys. Rev. B* **63**, 134409 (2001).
- [45] G. Misguich and B. Bernu, Specific heat of the $S = \frac{1}{2}$ Heisenberg model on the kagome lattice: High-temperature series expansion analysis, *Phys. Rev. B* **71**, 014417 (2005).
- [46] B. Bernu and C. Lhuillier, Spin Susceptibility of Quantum Magnets from High to Low Temperatures, *Phys. Rev. Lett.* **114**, 057201 (2015).
- [47] G. Misguich and P. Sindzingre, Magnetic susceptibility and specific heat of the spin-Heisenberg model on the kagome lattice and experimental data on $\text{ZnCu}_3(\text{OH})_6\text{Cl}_2$, *Eur. Phys. J. B* **59**, 305 (2007).
- [48] H.-J. Schmidt, A. Hauser, A. Lohmann, and J. Richter, Interpolation between low and high temperatures of the specific heat for spin systems, *Phys. Rev. E* **95**, 042110 (2017).
- [49] O. Derzhko, T. Hutak, T. Krokhnalskii, J. Schnack, and J. Richter, Adapting Planck's route to investigate the thermodynamics of the spin-half pyrochlore Heisenberg antiferromagnet, *Phys. Rev. B* **101**, 174426 (2020).
- [50] V. Grison, P. Viot, B. Bernu, and L. Messio, Emergent Potts order in the kagome $J_1 - J_3$ Heisenberg model, *Phys. Rev. B* **102**, 214424 (2020).
- [51] T. Hutak, T. Krokhnalskii, O. Derzhko, and J. Richter, Spin-half Heisenberg antiferromagnet on a symmetric sawtooth chain: rotation-invariant Green's functions and high-temperature series, *Eur. Phys. J. B* **96**, 50 (2023).
- [52] T. Hutak, T. Krokhnalskii, J. Schnack, J. Richter, and O. Derzhko, Thermodynamics of the $S = \frac{1}{2}$ hyperkagome-lattice Heisenberg antiferromagnet, *Phys. Rev. B* **110**, 054428 (2024).
- [53] P. Prelovšek, K. Morita, T. Tohyama, and J. Herbrych, Vanishing Wilson ratio as the hallmark of quantum spin-liquid models, *Phys. Rev. Res.* **2**, 023024 (2020).
- [54] P. Prelovšek and J. Kokalj, Similarity of thermodynamic properties of the Heisenberg model on triangular and kagome lattices, *Phys. Rev. B* **101**, 075105 (2020).
- [55] K. Seki and S. Yunoki, Thermodynamic properties of an $S = \frac{1}{2}$ ring-exchange model on the triangular lattice, *Phys. Rev. B* **101**, 235115 (2020).
- [56] J. Richter, O. Derzhko, and J. Schnack, Thermodynamics of the spin-half square kagome lattice antiferromagnet, *Phys. Rev. B* **105**, 144427 (2022).
- [57] J. Richter and J. Schnack, Magnetism of the $S = \frac{1}{2} J_1 - J_2$ square-kagome lattice antiferromagnet, *Phys. Rev. B* **107**, 245115 (2023).
- [58] P. Coleman, *Introduction to many-body physics* (Cambridge University Press, 2015).
- [59] M. Takahashi, Modified spin-wave theory of a square-lattice antiferromagnet, *Phys. Rev. B* **40**, 2494 (1989).